World Journal of Engineering Research
Print ISSN: 2959-9865
Online ISSN: 2959-9873
DOI: https://doi.org/10.61784/wjer3125

A TRAJECTORY PLANNING METHOD FOR FIXED-WING AIRCRAFT IN STATIC NO-FLY ZONE ENVIRONMENTS

ChengYi Zhang, Yang Guo*, Jia Liu, JiMao Sang
Rocket Force University of Engineering, Xi'an 710025, Shaanxi, China.
**Corresponding Author: Yang Guo*

Abstract: To address the difficulty of simultaneously satisfying heading continuity, minimum turning-radius constraints, and safe obstacle avoidance in trajectory planning for fixed-wing aircraft operating in static no-fly zone (NFZ) environments, a horizontal trajectory planning model is formulated by incorporating position, heading, curvature constraints, and safety margins around NFZs. A planning method combining weighted kinematic A* with Dubins terminal connection is then proposed. The method jointly represents planar position and heading angle as the search state and expands nodes using constant-curvature motion primitives that satisfy the prescribed curvature constraints. A weighted Dubins distance is employed to guide the search toward the target, while a Dubins curve is used within the target neighborhood to connect the current state to the desired terminal state. Simulation results demonstrate that, in scenarios involving multiple circular NFZs, the proposed method can generate continuous collision-free trajectories that satisfy the prescribed initial and terminal headings, safety-clearance requirements, and minimum turning-radius constraints. The resulting trajectory length increases only moderately relative to the straight-line distance, while the explored nodes are primarily concentrated near feasible passages. These results validate the effectiveness of the proposed method for trajectory planning of fixed-wing aircraft in static NFZ environments.
Keywords: Fixed-wing aircraft; Trajectory planning; Weighted kinematic A*; Dubins curve; No-fly zone

1 INTRODUCTION

In recent years, unmanned aerial vehicles (UAVs) have been widely employed in remote sensing and mapping, disaster inspection, target search, low-altitude logistics, border patrol, and emergency rescue. Trajectory planning has consequently become a fundamental capability supporting autonomous operation and mission execution. Aggarwal and Kumar noted that the primary objective of trajectory planning is to generate a feasible path between a specified start point and destination while satisfying safety, reachability, and mission requirements, and that its performance directly affects mission efficiency and operational reliability of UAV systems [1]. Ait Saadi et al. systematically reviewed optimization methods for UAV path planning and concluded that practical planning problems typically involve environmental constraints, vehicle performance limitations, and trade-offs among multiple objectives, making them difficult to address using a single simplified model [2]. Husnain et al. further pointed out that, with increasing levels of UAV autonomy, path-planning research is progressively shifting from static, low-dimensional, and idealized settings toward autonomous decision-making and real-time planning in complex environments [3].

Existing UAV trajectory-planning methods can generally be categorized into graph-search, sampling-based, intelligent optimization, and learning-based approaches. Gugan and Haque reviewed environmental modeling and path-generation techniques for autonomous UAV path planning and highlighted substantial differences among algorithms in terms of computational efficiency, path quality, environmental adaptability, and implementation complexity [4]. From the perspective of remote-sensing applications, Debnath et al. and Jiang et al. summarized UAV path-planning and obstacle-avoidance methods and identified the integration of global planning with local obstacle avoidance as an important direction for improving adaptability to complex missions [5-6].

For fixed-wing aircraft, trajectory planning cannot be treated simply as a two-dimensional shortest-path problem. Fixed-wing aircraft generally must maintain forward motion and, unlike multirotor platforms, cannot hover or turn in place. Their trajectories must therefore satisfy kinematic constraints such as minimum turning radius, heading continuity, and bounded curvature. Gao et al. and Du et al. proposed feasible trajectory-planning methods for fixed-wing UAVs by combining adaptive step-size search with online motion-primitive expansion, emphasizing that the dynamic and control characteristics of fixed-wing platforms significantly affect trajectory trackability [7-8]. Huang et al. introduced an improved bidirectional rapidly-exploring random tree (RRT) algorithm together with a three-dimensional Dubins method for low-altitude penetration path planning of fixed-wing aircraft, demonstrating that search efficiency and kinematic feasibility should be considered jointly [9]. From the perspective of six-degree-of-freedom UAV path planning and trajectory-tracking control, Wang et al. indicated that insufficient consideration of vehicle dynamics during planning may compromise subsequent tracking-control performance [10].

In complex constrained environments, no-fly zones (NFZs) constitute a common and important class of hard constraints in UAV trajectory planning. Chai et al. and Fan et al. proposed multi-strategy differential evolution algorithms for three-dimensional UAV path planning in complex environments and incorporated radar threats, firepower threats, NFZs, and other factors into mission-environment modeling, showing that threat sources can substantially reduce the feasible search space [11-12]. Zhou et al. and Jiang et al. developed NFZ identification methods for UAV delivery under urban wind conditions, indicating that NFZs may arise not only from fixed obstacles or mission restrictions but also from dynamically defined environmental risks [13-14].

Against this background, this paper considers horizontal trajectory planning for a single fixed-wing aircraft operating in a static environment containing multiple NFZs and formulates a planning model incorporating position, heading, NFZ safety margins, and minimum turning-radius constraints. To address the heading discontinuities and curvature-infeasible paths that can arise from conventional two-dimensional grid-based search, planar position and heading angle are jointly incorporated into the search state. A weighted kinematic A* algorithm is then employed to expand constant-curvature motion primitives satisfying the prescribed curvature constraints, while Dubins curves are used to construct both the heuristic cost and the terminal connection. Finally, MATLAB simulations in scenarios containing multiple circular NFZs, together with quantitative data analysis, are conducted to evaluate the capability of the proposed method to generate safe and kinematically feasible trajectories.

2 PROBLEM FORMULATION

2.1 Flight Mission and Kinematic Model

This paper considers horizontal trajectory planning for a single fixed-wing aircraft operating in an environment containing static no-fly zones. The aircraft departs from waypoint A and flies toward waypoint B. The initial and terminal headings are directly specified by the mission requirements. The planned trajectory must avoid all no-fly zones within the mission area while satisfying the minimum turning-radius constraint.

A fixed-wing aircraft must maintain forward motion and cannot stop at an arbitrary position or change its heading in place as permitted by a generic point-mass model. If the search is performed only in the two-dimensional position space, the resulting piecewise-linear path generally contains discontinuous heading changes, and the equivalent curvature at turning points may exceed the maneuvering capability of the aircraft. Therefore, both planar position and heading are incorporated into the planning state.

Taking the trajectory arc length s as the independent variable, the aircraft state is expressed as

$$\mathbf{q}(s) = [x(s)\ y(s)\ \psi(s)]^{\mathrm{T}}, s \in [0, L] \tag{1}$$

where $x(s)$ and $y(s)$ denote the eastward and northward positions, respectively, in the local coordinate system, $\psi(s)$ denotes the heading angle, and L is the total length of the complete trajectory. In this paper, the eastward direction is defined as zero heading, and the heading angle increases counterclockwise; therefore, the northward direction corresponds to $\psi = \pi/2$. The initial and terminal states are respectively expressed as

$$\mathbf{q}_{\mathrm{s}} = [x_{\mathrm{s}}\ y_{\mathrm{s}}\ \psi_{\mathrm{s}}]^{\mathrm{T}}, \mathbf{q}_{\mathrm{g}} = \left[x_{\mathrm{g}}\ y_{\mathrm{g}}\ \psi_{\mathrm{g}}\right]^{\mathrm{T}}, \mathbf{q}(0) = \mathbf{q}_{\mathrm{s}}, \mathbf{q}(L) = \mathbf{q}_{\mathrm{g}} \tag{2}$$

where $(x_{\mathrm{s}}, y_{\mathrm{s}})$ and $\left(x_{\mathrm{g}}, y_{\mathrm{g}}\right)$ denote the local planar coordinates of the starting and terminal points, respectively, while ψ_{s} and ψ_{g} denote the initial and terminal heading angles, respectively. The conditions given in Eq. (2) are not merely positional reachability constraints. The aircraft must also satisfy the prescribed arrival direction upon reaching the terminal point. If the trajectory is required only to pass through the target position while the terminal heading is ignored, the planner may approach the destination from an unsuitable direction, making it difficult to maintain continuity with the subsequent flight segment. Therefore, the terminal heading constraint should be incorporated into both cost estimation and goal connection from the beginning of the search rather than corrected separately after planning is completed.

The waypoints and no-fly-zone centers provided as engineering inputs are specified in longitude and latitude. Because longitude and latitude are defined on a spherical surface, planar Euclidean distance cannot be directly used to characterize relative positions over spatial scales of several hundred kilometers. To provide a unified representation for motion propagation and obstacle detection, a local east–north coordinate system is established using the starting point A as the projection center. Let the longitude and latitude of the projection center be (λ_0, φ_0) and those of a point to be transformed be (λ, φ). The azimuthal equidistant projection is then given by

$$\begin{cases} c = \arccos[\sin\varphi_0 \sin\varphi + \cos\varphi_0 \cos\varphi \cos(\lambda - \lambda_0)], \\ k = \begin{cases} c/\sin c, & c \neq 0, \\ 1, & c = 0, \end{cases} \\ x = R_{\mathrm{e}} k \cos\varphi \sin(\lambda - \lambda_0), \\ y = R_{\mathrm{e}} k[\cos\varphi_0 \sin\varphi - \sin\varphi_0 \cos\varphi \cos(\lambda - \lambda_0)]. \end{cases} \tag{3}$$

where R_{e} denotes the mean Earth radius, c is the spherical angular distance between the projection center and the point to be transformed, k is the projection scale factor, and x and y are the projected eastward and northward coordinates, respectively. When the point to be transformed coincides with the projection center, $k = 1$ is assigned to avoid division by zero in numerical computation. The azimuthal equidistant projection preserves the distance and azimuth relationships from the projection center to other locations. In this paper, waypoint A is used as the projection center, so the starting point corresponds to the origin of the local coordinate system. The terminal point and the centers of all no-fly zones are represented relative to this origin. This treatment preserves the principal geographic relationships within the mission area while allowing circular no-fly zones to remain represented as circles in the planar coordinate system. After trajectory planning is completed, the local trajectory is transformed back into longitude and latitude through the inverse projection for visualization and data output.

Only horizontal motion at a fixed altitude is considered. The aircraft flies forward at a prescribed cruise speed and adjusts its heading by varying the trajectory curvature. With arc length as the independent variable, the kinematic model is expressed as

$$\begin{cases} \frac{\mathrm{d}x}{\mathrm{d}s} = \cos\psi(s), \\ \frac{\mathrm{d}y}{\mathrm{d}s} = \sin\psi(s), \\ \frac{\mathrm{d}\psi}{\mathrm{d}s} = \kappa(s). \end{cases} \tag{4}$$

where $\kappa(s)$ denotes the trajectory curvature at arc-length position s. A positive curvature corresponds to a left turn, a negative curvature corresponds to a right turn, and zero curvature corresponds to straight-line flight. Arc-length parameterization directly relates changes in position to changes in heading. As long as the cruise speed remains constant, the geometric shape of the trajectory can be determined independently of flight time. Let the minimum turning radius of the aircraft be $R_{\min}$. The curvature constraint is then given by

$$|\kappa(s)| \le \kappa_{\max} = \frac{1}{R_{\min}}, \forall s \in [0, L] \tag{5}$$

where $\kappa_{\max}$ denotes the maximum allowable trajectory curvature. A larger minimum turning radius reduces the heading change achievable per unit distance traveled and increases the lateral space required to maneuver around obstacles. Under the assumption of constant cruise speed, the relationship between trajectory length and estimated flight time is

$$L = \int_0^{T_\mathrm{f}} v_\mathrm{c}\mathrm{d}t = v_\mathrm{c}T_\mathrm{f},\ T_\mathrm{f} = \frac{L}{v_\mathrm{c}} \tag{6}$$

where v_c denotes the cruise speed and T_f denotes the estimated flight time. Therefore, using trajectory length as the search cost is also equivalent to minimizing flight time under the current constant-speed assumption.

2.2 No-Fly Zone Constraints and Optimization Problem

Assume that the mission area contains a total of N_o static circular NFZs. The ith NFZ is represented as

$$\mathcal{O}_i = \{\mathbf{p} \in \mathbb{R}^2 \mid \|\mathbf{p} - \mathbf{o}_i\|_2 \le r_i\},\ \mathbf{o}_i = \left[o_{x,i}\ o_{y,i}\right]^\mathrm{T} \tag{7}$$

where $\mathbf{p} = [x, y]^\mathrm{T}$ denotes the planar position, $\mathbf{o}_i$ denotes the center of the ith NFZ, $o_{x,i}$ and $o_{y,i}$ are its eastward and northward coordinates, respectively, r_i is the original radius of the NFZ, N_o is the total number of NFZs, and $|\cdot|_2$ denotes the Euclidean norm. The circular representation provides a direct description of the center location and spatial extent of each NFZ, while collision detection requires only the distance between a trajectory point and the corresponding center. This representation also facilitates the incorporation of a safety margin into the original radius. For irregularly shaped restricted regions, future extensions may approximate them using combinations of multiple circular regions or replace the collision-detection module with a polygon-based method, without modifying the search-state definition or the kinematic propagation procedure.

If the trajectory is required only to avoid the original NFZs, the resulting path may pass arbitrarily close to their boundaries. To account for positioning errors, trajectory discretization errors, and tracking deviations during actual flight, a uniform safety margin is imposed on each NFZ:

$$r_i^{\mathrm{eff}} = r_i + r_\mathrm{m},\ \mathcal{O}_i^{\mathrm{eff}} = \left\{\mathbf{p} \in \mathbb{R}^2 \mid \|\mathbf{p} - \mathbf{o}_i\|_2 \le r_i^{\mathrm{eff}}\right\} \tag{8}$$

where r_m denotes the safety margin, r_i^{eff} denotes the effective radius of the ith NFZ, and $\mathcal{O}_i^{\mathrm{eff}}$ denotes the safety-expanded NFZ. After obstacle inflation, the aircraft is still modeled as a point mass, while the required separation distance is incorporated into the obstacle boundary. No differentiated weights or risk levels are assigned to individual NFZs; instead, the same margin parameter is applied to all restricted regions. Accordingly, the safety margin represents a uniform minimum separation distance, and the complete trajectory must satisfy

$$\|\mathbf{p}(s) - \mathbf{o}_i\|_2 > r_i + r_\mathrm{m}, \mathbf{p}(s) = [x(s)\ y(s)]^\mathrm{T}, \forall s \in [0, L], i = 1, ..., N_\mathrm{o} \tag{9}$$

where $\mathbf{p}(s)$ denotes the two-dimensional trajectory position at arc length s. In the numerical implementation, points located exactly on the effective-radius boundary are treated as collision points; therefore, a strict inequality is adopted.

The NFZ constraint is treated as a hard constraint in this problem. The search cost does not increase continuously as the trajectory approaches an NFZ. As long as a motion primitive does not enter an expanded NFZ, it remains admissible for the search. This treatment preserves a clear interpretation of the cost function, but it also means that, among multiple collision-free trajectories, the planner does not explicitly favor trajectories with greater clearance. Therefore, the safety level is evaluated separately after planning using the minimum clearance. The minimum clearance at a given trajectory position and that of the complete trajectory are defined as

$$d_{\min}(s) = \min_{1 \le i \le N_\mathrm{o}}[\|\mathbf{p}(s) - \mathbf{o}_i\|_2 - r_i],\ D_{\min} = \min_{s \in [0, L]} d_{\min}(s) \tag{10}$$

where $d_{\min}(s)$ denotes the minimum distance from the current trajectory position to the boundaries of all original NFZs, and $D_{\min}$ denotes the minimum clearance along the complete trajectory. Because the original radius r_i is subtracted in this definition, satisfying $D_{\min} \ge r_\mathrm{m}$ indicates that the trajectory maintains the prescribed safety margin.

Eq. (9) requires the entire continuous trajectory to remain collision-free, whereas a numerical implementation can examine only a finite number of sampled points. A smaller collision-checking interval provides a closer approximation to the continuous constraint. If the interval is excessively large, however, a short segment of an arc may penetrate an NFZ without being detected at the sampled points. The planner must also operate within a finite search region. The search region is defined to encompass the initial point, terminal point, and all effective NFZs, with an additional boundary margin in all directions:

$$\begin{cases} x_{\min} = \min\left(x_{\mathrm{s}}, x_{\mathrm{g}}, \min\limits_{i}\{o_{x,i} - r_i^{\mathrm{eff}}\}\right) - r_{\mathrm{b}}, \\ x_{\max} = \max\left(x_{\mathrm{s}}, x_{\mathrm{g}}, \max\limits_{i}\{o_{x,i} + r_i^{\mathrm{eff}}\}\right) + r_{\mathrm{b}}, \\ y_{\min} = \min\left(y_{\mathrm{s}}, y_{\mathrm{g}}, \min\limits_{i}\{o_{y,i} - r_i^{\mathrm{eff}}\}\right) - r_{\mathrm{b}}, \\ y_{\max} = \max\left(y_{\mathrm{s}}, y_{\mathrm{g}}, \max\limits_{i}\{o_{y,i} + r_i^{\mathrm{eff}}\}\right) + r_{\mathrm{b}} \end{cases} \tag{11}$$

where $x_{\min}$, $x_{\max}$, $y_{\min}$, and $y_{\max}$ denote the boundaries of the rectangular search region, and r_{b} denotes the outward boundary margin. The finite search region is not a physical constraint imposed by the flight mission itself, but rather a numerical setting introduced to limit computational complexity. If the boundary margin is too small, feasible trajectories requiring large detours may be artificially truncated. Conversely, if the search region is excessively large, the planner may generate a substantial number of nodes in areas with little relevance to the mission. In practical implementation, the bounding region containing the initial point, terminal point, and all effective NFZs is used as the base search area, followed by the addition of a uniform margin. This strategy avoids unnecessarily restricting the principal detour directions in most scenarios. The search-region and endpoint-safety conditions are expressed as

$$\mathcal{B} = [x_{\min}, x_{\max}] \times [y_{\min}, y_{\max}], \mathbf{p}(s) \in \mathcal{B}, \mathbf{q}_{\mathrm{s}}, \mathbf{q}_{\mathrm{g}} \notin \bigcup_{i=1}^{N_{\mathrm{o}}} \mathcal{O}_i^{\mathrm{eff}} \tag{12}$$

where $\mathcal{B}$ denotes the rectangular search region and $\cup$ denotes the union of all effective NFZs. If either the initial point or the terminal point lies within any effective NFZ, the algorithm terminates during initialization and returns a planning failure.

The trajectory length is adopted as the optimization objective. Under arc-length parameterization, the cost is given by

$$J(\mathbf{q}) = L = \int_0^L \sqrt{\left(\frac{\mathrm{d}x}{\mathrm{d}s}\right)^2 + \left(\frac{\mathrm{d}y}{\mathrm{d}s}\right)^2}\mathrm{d}s, \sqrt{\left(\frac{\mathrm{d}x}{\mathrm{d}s}\right)^2 + \left(\frac{\mathrm{d}y}{\mathrm{d}s}\right)^2} = 1 \tag{13}$$

where $J(\mathbf{q})$ denotes the cost of a candidate trajectory. Because s is the arc-length parameter, the magnitude of the position derivative is identically equal to 1, and the integral therefore yields the total trajectory length. Combining the above conditions, the trajectory-planning problem is formulated as

$$\begin{aligned} &\min_{\mathbf{q}(\cdot)} \ L, \\ &\text{s.t.} \ \begin{cases} x'(s) = \cos\psi(s) \\ y'(s) = \sin\psi(s) \\ \psi'(s) = \kappa(s) \end{cases} \\ &|\kappa(s)| \le 1/R_{\min} \\ &\mathbf{q}(0) = \mathbf{q}_{\mathrm{s}}, \mathbf{q}(L) = \mathbf{q}_{\mathrm{g}} \\ &\|\mathbf{p}(s) - \mathbf{o}_i\|_2 > r_i + r_{\mathrm{m}}, \ i = 1, \dots, N_{\mathrm{o}} \\ &\mathbf{p}(s) \in \mathcal{B}, \forall s \in [0, L] \end{aligned} \tag{14}$$

where $\mathbf{q}(\cdot)$ denotes the state trajectory to be determined, and $x'(s)$, $y'(s)$, and $\psi'(s)$ denote the derivatives of the corresponding state variables with respect to arc length. This problem cannot be reduced to a conventional two-dimensional grid-based shortest-path problem. Heading is itself a state variable, and arriving at the same position with different headings leads to different sets of subsequently reachable states. Moreover, the curvature constraint restricts how neighboring states can be connected. Accordingly, a kinematic A* search is employed to identify feasible passages between NFZs, and a Dubins curve is used near the target to complete the terminal-state connection.

3 METHODOLOGY

3.1 Weighted Kinematic A* Search

The search is performed in a joint position–heading state space, with each planning node represented as $\mathbf{q} = (x, y, \psi)$. Continuous position and heading information are retained for each node, while a discrete grid is used for duplicate-state identification and cost-based pruning. Let the positional grid resolution be Δ_{g} and divide the heading space into N_ψ intervals. The state indices and the corresponding discrete state key are defined as

$$\begin{cases} \mathcal{M}(\psi) = \psi - 2\pi\left\lfloor\frac{\psi}{2\pi}\right\rfloor \\ i_x = \max\left[0, \left\lfloor\frac{x - x_{\min}}{\Delta_{\mathrm{g}}}\right\rfloor\right] \\ i_y = \max\left[0, \left\lfloor\frac{y - y_{\min}}{\Delta_{\mathrm{g}}}\right\rfloor\right] \\ i_\psi = \min\left[N_\psi - 1, \left\lfloor\frac{\mathcal{M}(\psi)}{2\pi}N_\psi\right\rfloor\right] \\ \mathcal{K}(\mathbf{q}) = (i_x, i_y, i_\psi) \end{cases} \tag{15}$$

where $\mathcal{M}(\psi)$ maps the heading angle into $[0, 2\pi)$, i_x, i_y, and i_ψ denote the eastward-position, northward-position, and heading indices, respectively, Δ_g is the positional resolution, N_ψ is the number of heading intervals, and $\mathcal{K}(\mathbf{q})$ denotes the discrete key associated with state $\mathbf{q}$. When multiple nodes are mapped to the same discrete state, only the node with the lower accumulated cost is retained:

$$g_\mathrm{best}\left(\mathcal{K}\left(\mathbf{q}'\right)\right) \leftarrow \begin{cases} g\left(\mathbf{q}'\right), & \mathcal{K}\left(\mathbf{q}'\right) \notin \mathcal{G} \text{ or } g\left(\mathbf{q}'\right) < g_\mathrm{best}\left(\mathcal{K}\left(\mathbf{q}'\right)\right) - \varepsilon, \\ g_\mathrm{best}\left(\mathcal{K}\left(\mathbf{q}'\right)\right), & \text{others} \end{cases} \tag{16}$$

where $\mathbf{q}'$ denotes a candidate node, $g\left(\mathbf{q}'\right)$ is the accumulated trajectory length from the initial state to that node, g_best is the minimum cost currently recorded for the corresponding discrete state, $\mathcal{G}$ denotes the set of previously recorded state keys, and ε is the tolerance used for floating-point comparisons.

Adjacent nodes are connected using constant-curvature motion primitives. Let the length of each primitive be l_p. The admissible curvature set is defined as

$$\mathcal{U}_\kappa = \frac{1}{R_\mathrm{min}}\left\{-1, -\frac{2}{3}, -\frac{1}{3}, 0, \frac{1}{3}, \frac{2}{3}, 1\right\} \tag{17}$$

where $\mathcal{U}_\kappa$ denotes the discrete curvature set and R_min is the minimum turning radius. Negative curvature corresponds to a right turn, positive curvature to a left turn, and zero curvature to straight-line flight. All motion primitives satisfy $|\kappa| \leq 1/R_\mathrm{min}$.

For the current node $\mathbf{q}_k = (x_k, y_k, \psi_k)$, propagation over a distance l_p with constant curvature κ yields the terminal state

$$\mathbf{q}_{k+1} = \begin{cases} \begin{bmatrix} x_k + l_\mathrm{p}\cos\psi_k \\ y_k + l_\mathrm{p}\sin\psi_k \\ \psi_k \end{bmatrix}, & |\kappa| < \varepsilon_\kappa, \\ \begin{bmatrix} x_k + \frac{\sin(\psi_k + \kappa l_\mathrm{p}) - \sin\psi_k}{\kappa} \\ y_k + \frac{-\cos(\psi_k + \kappa l_\mathrm{p}) + \cos\psi_k}{\kappa} \\ \mathcal{N}(\psi_k + \kappa l_\mathrm{p}) \end{bmatrix}, & |\kappa| \geq \varepsilon_\kappa. \end{cases} \tag{18}$$

where $\mathbf{q}_{k+1}$ denotes the terminal state of the motion primitive, ε_κ is the near-zero curvature threshold, and $\mathcal{N}(\cdot)$ normalizes the heading angle to $[-\pi, \pi)$. Straight-line propagation is used when the curvature is close to zero; otherwise, the analytical solution for a constant-curvature circular arc is applied.

Collision checking is performed along the entire motion primitive. Let the collision-checking interval be Δ_c. The sampling locations along a primitive are then given by

$$N_\mathrm{c} = \left\lceil\frac{l_\mathrm{p}}{\Delta_\mathrm{c}}\right\rceil, \; s_j = \min(j\Delta_\mathrm{c}, l_\mathrm{p}), \; j = 1, \dots, N_\mathrm{c} \tag{19}$$

where N_c denotes the number of collision-checking points and s_j denotes the location of the jth checking point. Let the NFZ safety threshold be d_safe. The acceptance condition for a candidate primitive is defined as

$$\mathcal{A}(\mathbf{q}_{k+1}) = \left\{\bigwedge_{j=1}^{N_\mathrm{c}}\bigwedge_{i=1}^{N_\mathrm{o}}\left[\left\|\mathbf{p}(s_j) - \mathbf{o}_i\right\|_2 - r_i > d_\mathrm{safe}\right]\right\} \wedge [\mathbf{p}_{k+1} \in \mathcal{B}] \tag{20}$$

where $\mathcal{A}(\mathbf{q}_{k+1})$ denotes the acceptance function for the candidate primitive, $\mathbf{p}(s_j)$ is the position of the jth collision-checking point, $\mathbf{o}_i$ and r_i denote the center and radius of the ith NFZ, respectively, N_o is the number of NFZs, $\mathbf{p}_{k+1}$ denotes the terminal position of the primitive, $\mathcal{B}$ is the search region, and $\wedge$ denotes logical conjunction.

Because all A* motion primitives have the same length, the accumulated node cost is given by

$$g(\mathbf{q}_\mathrm{s}) = 0, \; g(\mathbf{q}_{k+1}) = g(\mathbf{q}_k) + l_\mathrm{p}, \; g(\mathbf{q}_k) = kl_\mathrm{p} \tag{21}$$

where $g(\mathbf{q}_k)$ denotes the accumulated trajectory length from the initial state to node $\mathbf{q}_k$, and k is the number of motion primitives associated with that node. Candidate nodes that pass both collision checking and boundary checking are further subjected to duplicate-state pruning according to Eq. (16).

3.2 Dubins Heuristic, Terminal Connection, and Trajectory Generation

Euclidean distance reflects only the positional difference between two states and cannot account for the influence of the current heading on the remaining trajectory length. Therefore, the shortest Dubins distance under obstacle-free conditions is adopted as the heuristic cost. Consider two states to be connected, $\mathbf{q}_a = (x_a, y_a, \psi_a)$ and $\mathbf{q}_b = (x_b, y_b, \psi_b)$. Their relative configuration is normalized by the minimum turning radius as

$$\begin{cases} \Delta x = \frac{x_b - x_a}{R_\mathrm{min}}, \Delta y = \frac{y_b - y_a}{R_\mathrm{min}} \\ d = \sqrt{\Delta x^2 + \Delta y^2}, \theta = \mathcal{M}[\mathrm{atan2}(\Delta y, \Delta x)] \\ \alpha = \mathcal{M}(\psi_a - \theta), \beta = \mathcal{M}(\psi_b - \theta) \end{cases} \tag{22}$$

where Δx and Δy denote the normalized relative positions, d is the normalized distance, θ denotes the direction of the line connecting the two state positions, and α and β denote the initial and terminal headings relative to this direction, respectively. The candidate Dubins paths and the shortest Dubins distance are expressed as

$$\varSigma = \{\mathrm{LSL}, \mathrm{RSR}, \mathrm{LSR}, \mathrm{RSL}, \mathrm{RLR}, \mathrm{LRL}\}, L_\sigma = R_{\min}(t_\sigma + p_\sigma + q_\sigma), D_{\mathrm{D}} = \min_{\sigma \in \varSigma_{\mathrm{valid}}} L_\sigma \tag{23}$$

where $\varSigma$ denotes the set of six Dubins path types; L, R, and S represent left-turning, right-turning, and straight segments, respectively; t_σ, p_σ, and q_σ are the three normalized segment lengths associated with path type σ; $\varSigma_{\mathrm{valid}}$ denotes the set of feasible path types; L_σ is the length of a candidate Dubins path; and D_{D} denotes the shortest Dubins distance.

The evaluation function and node-selection rule for weighted A* are defined as

$$\begin{cases} h(\mathbf{q}) = D_{\mathrm{D}}(\mathbf{q}, \mathbf{q}_{\mathrm{g}}) \\ f(\mathbf{q}) = g(\mathbf{q}) + w_{\mathrm{h}} h(\mathbf{q}) \\ \mathbf{q}^* = \underset{\mathbf{q} \in \mathrm{OPEN}}{\operatorname{argmin}} f(\mathbf{q}) \end{cases} \tag{24}$$

where $h(\mathbf{q})$ denotes the heuristic cost from the current node to the goal state, $f(\mathbf{q})$ is the overall evaluation value, w_{h} is the heuristic weight, and $\mathbf{q}^*$ denotes the node selected for expansion. If the accumulated cost of a node removed from the OPEN set exceeds the best recorded cost associated with its discrete state, that node is discarded without further expansion. When $w_{\mathrm{h}} > 1$, the search is more strongly biased toward the goal, which can reduce the number of node expansions but no longer guarantees global optimality in the continuous state space. Accordingly, the resulting trajectory is regarded as a near-optimal feasible solution under the specified discretization parameters.

Fixed-length motion primitives generally cannot satisfy the target position and terminal heading exactly. Therefore, a terminal-connection distance D_{c} is introduced. Once the current node enters the target neighborhood, the shortest Dubins path from the current state to the goal state is computed and subsequently subjected to boundary and collision checks:

$$\begin{cases} d_{\mathrm{g}}(\mathbf{q}_k) = \sqrt{(x_k - x_{\mathrm{g}})^2 + (y_k - y_{\mathrm{g}})^2} \le D_{\mathrm{c}} \\ \mathcal{V}_{\mathrm{D}} = \bigwedge_{j=1}^{N_{\mathrm{D}}} \left\{ \mathbf{p}_{\mathrm{D}}(s_j) \in \mathcal{B} \wedge \bigwedge_{i=1}^{N_{\mathrm{o}}} \left[\left\| \mathbf{p}_{\mathrm{D}}(s_j) - \mathbf{o}_i \right\|_2 - r_i > d_{\mathrm{safe}} \right] \right\} \end{cases} \tag{25}$$

where $d_{\mathrm{g}}(\mathbf{q}_k)$ denotes the distance from the current node to the target position, D_{c} is the terminal-connection trigger distance, $\mathcal{V}_{\mathrm{D}}$ is the validity indicator for the terminal Dubins path, N_{D} denotes the number of collision-checking points along the terminal path, and $\mathbf{p}_{\mathrm{D}}(s_j)$ denotes the position of the jth checking point.

Among the six candidate Dubins path types, the algorithm performs collision checking only on the shortest one. If this path is infeasible, A* node expansion continues. If the terminal connection passes all validity checks, the parent-node chain is backtracked and the complete trajectory is generated as

$$\varGamma = \varGamma_{\mathrm{A*}} \oplus \varGamma_{\mathrm{D}}^*, \ \varGamma(0) = \mathbf{q}_{\mathrm{s}}, \ \varGamma(L) = \mathbf{q}_{\mathrm{g}} \tag{26}$$

where $\varGamma$ denotes the complete trajectory, $\varGamma_{\mathrm{A}}$ denotes the kinematic A search segment, $\varGamma_{\mathrm{D}}^*$ is the terminal Dubins path, and $\oplus$ denotes trajectory concatenation.

Suppose that the final output trajectory contains N_{p} discrete points. Its trajectory length and estimated flight time are calculated as

$$L_{\mathrm{out}} = \sum_{j=1}^{N_{\mathrm{p}}-1} \sqrt{(x_{j+1} - x_j)^2 + (y_{j+1} - y_j)^2}, \ T_{\mathrm{out}} = \frac{L_{\mathrm{out}}}{v_{\mathrm{c}}} \tag{27}$$

where N_{p} denotes the number of output trajectory points, L_{out} is the discrete trajectory length, T_{out} is the estimated flight time, and v_{c} denotes the cruise speed. The minimum clearance of the output trajectory is given by

$$d_j = \min_{1 \le i \le N_{\mathrm{o}}} \left[\sqrt{(x_j - o_{x,i})^2 + (y_j - o_{y,i})^2} - r_i \right], D_{\min}^{\mathrm{out}} = \min_{1 \le j \le N_{\mathrm{p}}} d_j \tag{28}$$

where d_j denotes the clearance between the jth trajectory point and the boundary of its nearest NFZ, and $D_{\min}^{\mathrm{out}}$ denotes the minimum discrete clearance over the complete trajectory. When $D_{\min}^{\mathrm{out}} \ge d_{\mathrm{safe}}$, the planned trajectory satisfies the prescribed safety threshold. During the search, all discovered but not yet expanded nodes are stored in the OPEN set. Upon successful planning, the algorithm outputs the complete trajectory together with the corresponding evaluation metrics. Planning is considered unsuccessful if the OPEN set becomes empty or the number of generated nodes reaches the prescribed upper limit.

4 SIMULATION VALIDATION

4.1 Simulation Environment and Parameter Settings

To evaluate the planning capability of the weighted kinematic A* method with Dubins terminal connection in an environment containing multiple NFZs, horizontal trajectory-planning simulations for a single aircraft were conducted in MATLAB. The mission requires the aircraft to fly from starting point A to terminal point B while avoiding four circular NFZs and simultaneously satisfying the prescribed initial heading, terminal heading, safety threshold, and minimum turning-radius constraints. The geographic coordinates of starting point A are 93.70°E and 36.82°N, while those of terminal point B are 87.71°E and 37.59°N. The initial and terminal headings are specified as 160° and 170°, respectively. The center coordinates and radii of the four NFZs are listed in Table 1.

Table 1 Simulation Scenario Configuration

NFZ	Longitude/°	Latitude/°	Radius/km
NFZ-1	92.5366	36.8511	30
NFZ-2	91.5380	37.6011	50
NFZ-3	89.7141	37.2652	40
NFZ-4	91.1738	36.8618	15

The minimum turning radius of the aircraft is set to 90 km, the cruise speed to 1870 m/s, and the flight altitude to 10 km. The NFZ safety threshold is set to 5 km, meaning that the planned trajectory must maintain a clearance of at least 5 km from the original boundary of every NFZ. The kinematic A* search uses motion primitives with a fixed length of 12 km. At each node, seven basic motion modes are considered for expansion: maximum right turn, medium right turn, slight right turn, straight flight, slight left turn, medium left turn, and maximum left turn. The positional grid resolution is set to 5 km, while the heading space is divided into 72 intervals, corresponding to a resolution of 5° per interval. The collision-checking interval is set to 0.8 km, and the final trajectory-output interval is set to 2 km. The heuristic weight of weighted A* is set to 1.25, the Dubins terminal-connection distance to 180 km, the maximum number of search nodes to 500,000, and the search-region boundary margin to 120 km. All simulations are performed using MATLAB R2024b.

4.2 Trajectory Planning Results and Constraint Verification

Figure 1 presents the planned trajectory in both the local planar coordinate system and the geographic coordinate system. In the local coordinate system, starting point A is taken as the origin, with the horizontal axis representing eastward distance and the vertical axis representing northward distance. The red regions indicate the original NFZs, while the orange dashed curves denote the safety-constraint boundaries corresponding to the 5 km safety threshold.

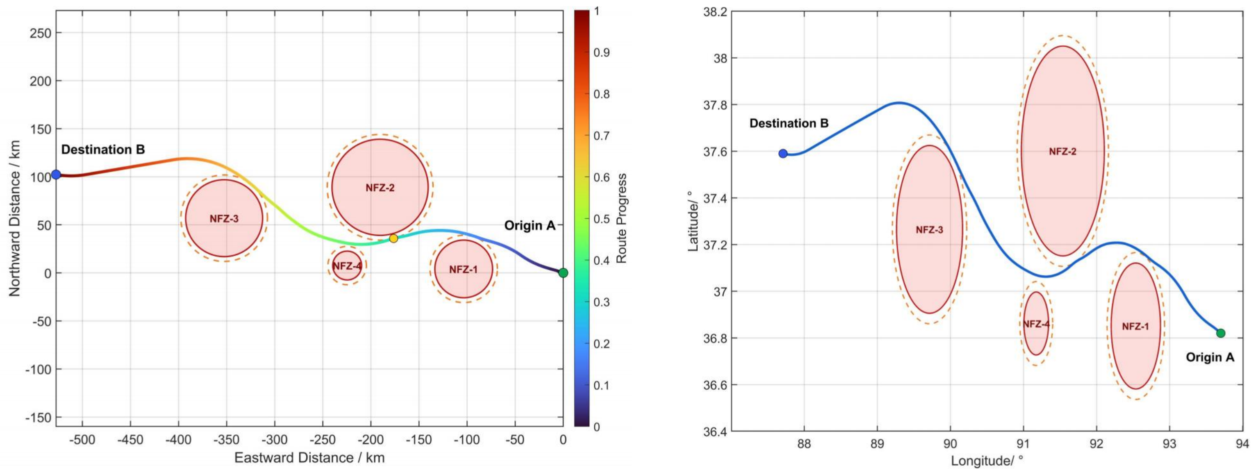

(a) Trajectory in the Local Planar Coordinate System (b) Trajectory in the Geographic Coordinate System

Figure 1 Planned Trajectory in a Multi-NFZ Environment

As shown in Figure 1(a), starting point A is located at the origin of the local coordinate system, while terminal point B is approximately 527.6 km west and 102.9 km north of A. After departure, the aircraft initially flies northwestward, passing to the north of NFZ-1 and NFZ-4 before detouring to the south of NFZ-2. During the latter half of the flight, the trajectory continues to adjust northwestward, passes to the north of NFZ-3, and eventually reaches terminal point B. The aircraft begins adjusting its heading before approaching the obstacle regions, and all turning segments extend over relatively large spatial scales, consistent with the prescribed minimum turning radius of 90 km. Figure 1(b) shows the same trajectory in the geographic coordinate system. After inverse projection of the local trajectory, the geographic locations of the starting point, terminal point, and all NFZs remain consistent with the original mission inputs. The geographic-coordinate representation illustrates the actual geographical course of the planned trajectory, whereas the local planar representation is more suitable for analyzing NFZ spacing, turning maneuvers, and safety clearance.

The straight-line planar distance between starting point A and terminal point B is approximately 537.5 km, whereas the planned trajectory has a length of 565.942 km. This corresponds to an additional travel distance of approximately 28.4 km, or an increase of approximately 5.3% relative to the straight-line distance. The additional distance is primarily attributable to detours around the NFZs, the minimum turning-radius constraint, and the terminal-heading adjustment.

To determine whether the planned trajectory satisfies the prescribed safety threshold, Figure 2 presents the safety clearance along the entire trajectory and the minimum passing clearance with respect to each NFZ. As shown in Figure 2(a), the clearance from the trajectory to the nearest NFZ boundary remains above the 5 km safety threshold throughout the flight. The global minimum clearance is 5.040 km and occurs at an accumulated trajectory length of approximately

190 km. This point corresponds to the segment in which the aircraft passes to the south of NFZ-2. Another pronounced local minimum in clearance occurs at an accumulated trajectory length of approximately 355 km, corresponding to the aircraft's detour to the north of NFZ-3. After the aircraft leaves the principal NFZ region, the clearance gradually increases and exceeds 100 km near the terminal point. These results indicate that the safety constraints primarily affect the middle portion of the trajectory, while relatively ample obstacle-free space is available near the starting and terminal points.

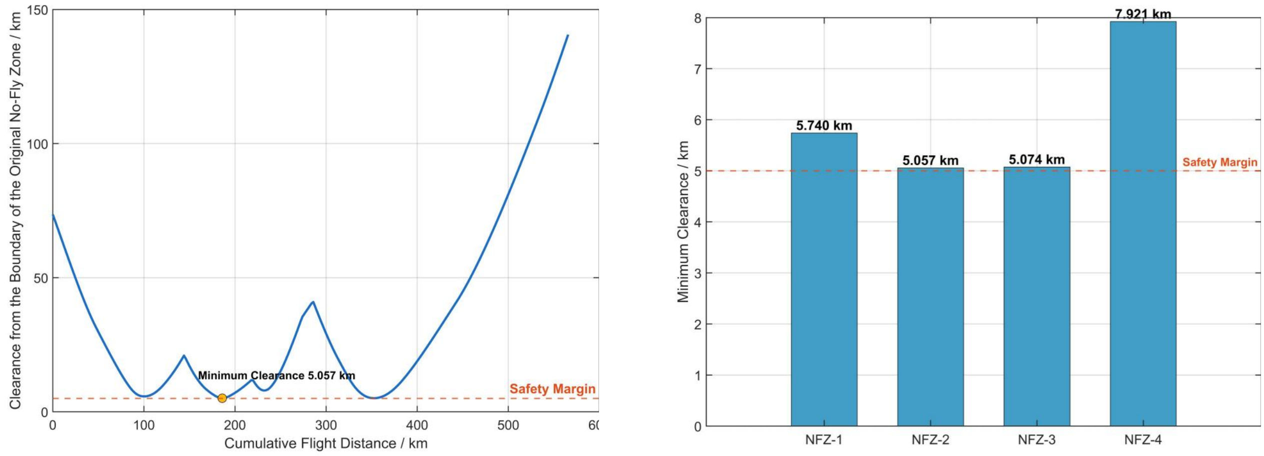

(a) Safety-Clearance Variation along the Complete Trajectory

(b) Minimum Passing Clearance for Each NFZ

Figure 2 Safety-Clearance Verification of the Planned Trajectory

Figure 2(b) further presents the minimum passing clearances with respect to the four NFZs. The minimum clearances from NFZ-1, NFZ-2, NFZ-3, and NFZ-4 are 11.939 km, 5.040 km, 5.178 km, and 12.962 km, respectively, all of which exceed the prescribed 5 km safety threshold. The minimum clearances associated with NFZ-2 and NFZ-3 are close to the safety threshold, indicating that these two NFZs are the primary obstacles governing the geometric shape of the planned trajectory. By contrast, the minimum passing clearances from NFZ-1 and NFZ-4 both exceed 11 km. Although these two NFZs influence the local flight direction, neither determines the global minimum clearance.

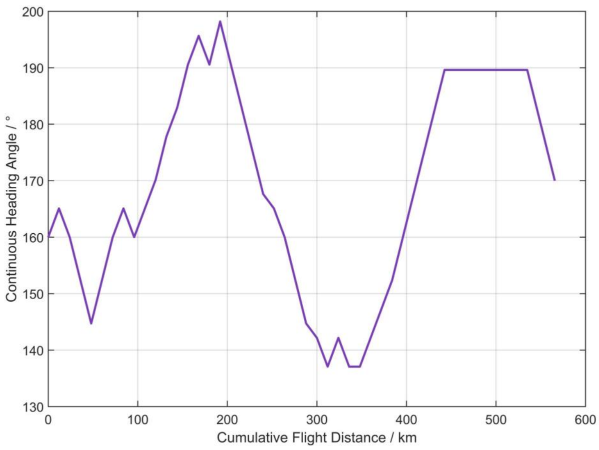

Figure 3 Kinematic-Constraint Verification of the Planned Trajectory

The variations in heading angle with accumulated trajectory length are shown in Figure 3. As illustrated in Figure 3, the trajectory starts with an initial heading of 160° and is adjusted progressively according to the spatial distribution of the NFZs during the detour process. The heading angle increases to approximately 200° during the first half of the trajectory and subsequently decreases to about 135°. After entering the terminal phase, the heading is adjusted again and eventually reaches the prescribed terminal heading of 170°. The heading profile remains continuous throughout the entire trajectory, with no instantaneous discontinuities. Changes in the slope of the heading curve at several locations correspond to transitions between different constant-curvature motion primitives. The nearly horizontal segment at approximately 189° in the middle-to-late portion of the trajectory indicates approximately straight flight, while the decrease in heading from about 189° to 170° near the end corresponds to the right-turning segment of the Dubins terminal connection.

The curvature profile remains within the prescribed upper and lower turning limits throughout the trajectory, indicating that the turning radius of the complete trajectory is never smaller than the specified minimum value of 90 km. Some trajectory segments reach the upper or lower curvature limits, demonstrating that the aircraft employs the maximum allowable curvature during obstacle avoidance. The curvature primarily takes seven discrete levels corresponding to maximum right turn, medium right turn, slight right turn, straight flight, slight left turn, medium left turn, and maximum left turn, consistent with the motion-primitive configuration used in the kinematic A* search. The terminal Dubins path consists of maximum-curvature left-turning or right-turning segments and straight segments to complete the connection to the goal state.

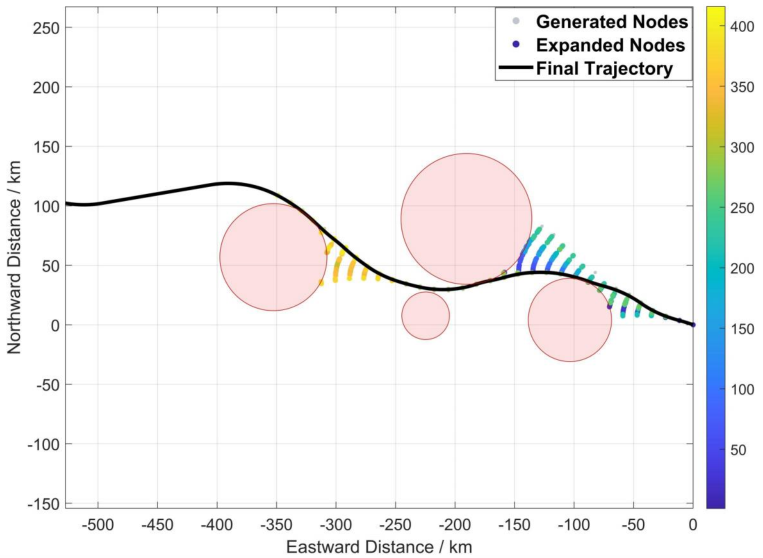

Figure 4 Spatial Distribution of A* Search Nodes

Figure 4 shows the spatial distribution of A* search nodes in the local coordinate system. The scattered points represent nodes generated or expanded during the search, with their colors indicating the node-expansion order, while the black curve represents the final planned trajectory. The search nodes are concentrated primarily within feasible corridors between starting point A and terminal point B rather than being uniformly distributed over the entire search region. Near the starting point, nodes expand along different curvature directions, forming multiple short-range candidate branches. As the search progresses, the nodes gradually become concentrated in regions with lower evaluation costs.

Search branches are relatively dense near NFZ-1 and NFZ-2. After departing from the starting point, the aircraft must establish a connection passing to the north of NFZ-1 and to the south of NFZ-2 while satisfying the minimum turning-radius constraint. Consequently, the planner generates multiple candidate nodes with different positions and headings. Some nodes are not expanded further because they either approach the NFZ safety boundaries or have relatively high overall evaluation costs. Near NFZ-3, the search has already converged toward a principal detour direction passing to its north, resulting in a more concentrated node distribution. The final trajectory lies within a continuous corridor formed by high-priority search nodes. A total of 608 nodes are expanded during the entire search process, which is substantially below the prescribed upper limit of 500,000 nodes.

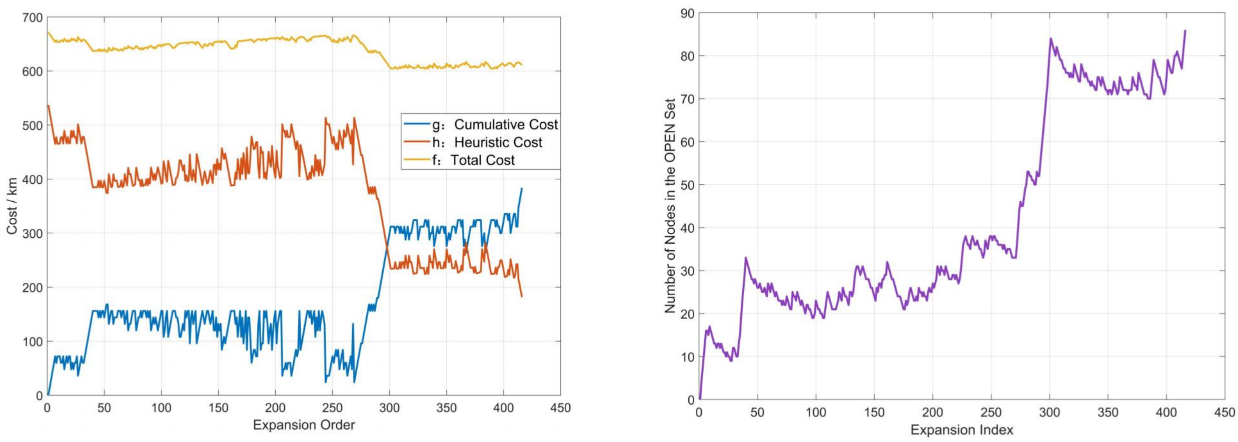

(a) Evolution of Search Costs (b) Variation in OPEN-Set Size

Figure 5 Evolution of A* Search Costs and OPEN-Set Size

As shown in Figure 5(a), different expanded nodes may belong to different search branches; therefore, the three cost curves do not vary monotonically with the node index. For approximately the first 500 expanded nodes, the overall evaluation cost is mainly distributed between 640 and 670 km, indicating that multiple candidate paths with similar evaluation values coexist in the OPEN set. After approximately the 500th expanded node, the accumulated cost increases noticeably while the heuristic cost decreases rapidly, indicating that the currently expanded nodes are approaching the target region along a feasible corridor. The overall evaluation cost subsequently decreases to approximately 610 km, at which point a Dubins terminal connection satisfying the safety requirements is identified.

The heuristic cost does not decrease to zero when the search terminates. This is because the A* search nodes are not required to reach terminal point B directly. Once a node enters the 180 km terminal-connection region and the shortest Dubins path passes the safety checks, A* expansion terminates and the Dubins path completes the remaining trajectory segment. Figure 5(b) shows that the size of the OPEN set remains at approximately 10–35 nodes during the early stage of the search and gradually increases as additional candidate branches are generated. During the later stage, the OPEN-set size increases to approximately 100–110 nodes. When planning succeeds, the OPEN set still contains unexpanded nodes, indicating that the search terminates because a valid terminal connection has been found rather than because the candidate state space has been exhausted.

The above results demonstrate that, under the current simulation scenario and parameter settings, the planner can generate a continuous collision-free trajectory from starting point A to terminal point B. The global minimum clearance remains above the prescribed 5 km safety threshold, the normalized curvature stays within the allowable range, and both the initial and terminal heading requirements are satisfied. Moreover, the search nodes are concentrated primarily near the NFZs and within feasible corridors connecting the initial and terminal points, without extensive ineffective expansion over the search region.

5 CONCLUSION

This paper addressed horizontal trajectory planning for fixed-wing aircraft operating in environments with static no-fly zones. A planning model incorporating position, heading, minimum turning radius, and NFZ safety margins was formulated, and a trajectory-generation method combining weighted kinematic A* with Dubins terminal connection was proposed. The method incorporates heading into the search state, expands nodes using constant-curvature motion primitives, and employs Dubins distance both to guide the search and to complete the terminal connection. Consequently, the generated trajectories can simultaneously satisfy obstacle-avoidance requirements, heading continuity, and curvature constraints.

Simulation results demonstrate that, in scenarios containing multiple NFZs, the proposed method can generate continuous and feasible detour trajectories from the initial point to the terminal point. The resulting trajectories satisfy the prescribed safety-clearance, minimum turning-radius, and initial and terminal heading constraints. In addition, the search nodes are concentrated primarily around feasible corridors, indicating effective search guidance and satisfactory planning performance. Future work will consider dynamic obstacles, wind-field disturbances, altitude variations, multi-aircraft coordination, and comparative validation across a broader range of scenarios to further improve the adaptability of the method to complex real-world airspace and enhance its potential for practical implementation.

COMPETING INTERESTS

The authors have no relevant financial or non-financial interests to disclose.

FUNDING

This work was supported by the National Natural Science Foundation of China under Grant No. 62473375, and Shaanxi Provincial Outstanding Youth Science Fund under Grant No. 2022-JC-42.

REFERENCES

[1] Aggarwal S, Kumar N. Path planning techniques for unmanned aerial vehicles: A review, solutions, and challenges. Computer Communications, 2020, 149: 270-299. DOI: 10.1016/j.comcom.2019.10.014.

[2] Ait Saadi A, Soukane A, Meraihi Y, et al. UAV path planning using optimization approaches: A survey. Archives of Computational Methods in Engineering, 2022, 29(6): 4233-4284. DOI: 10.1007/s11831-022-09742-7.

[3] Ul Husnain A, Mokhtar N, Mohamed Shah N, et al. A systematic literature review on autonomous path planning of unmanned aerial vehicles. Drones, 2023, 7(2): 118. DOI: 10.3390/drones7020118.

[4] Gugan G, Haque A. Path planning for autonomous drones: Challenges and future directions. Drones, 2023, 7(3): 169. DOI: 10.3390/drones7030169.

[5] Debnath D, Vanegas F, Sandino J, et al. A review of UAV path-planning algorithms and obstacle avoidance methods for remote sensing applications. Remote Sensing, 2024, 16(21): 4019. DOI: 10.3390/rs16214019.

[6] Jiang Y, Xu X X, Zheng M Y, et al. Evolutionary computation for unmanned aerial vehicle path planning: A survey. Artificial Intelligence Review, 2024, 57: 267. DOI: 10.1007/s10462-024-10913-0.

[7] Gao H, Jia Y, Qin Q, et al. Integrating just-in-time expansion primitives and an adaptive variable-step-size mechanism for feasible path planning of fixed-wing UAVs. Chinese Journal of Aeronautics, 2025, 38(12): 103566. DOI: 10.1016/j.cja.2025.103566.

[8] Du H, You M, Zhao X. Globally guided deep V-network-based motion planning algorithm for fixed-wing unmanned aerial vehicles. Sensors, 2024, 24(12): 3984. DOI: 10.3390/s24123984.

[9] Huang H, Shang Y, Liu X, et al. An improved Bi-RRT*-based path planning algorithm with adaptive search strategy assignment mechanism for ultra-low-altitude penetration of fixed-wing aircraft. Aerospace Science and Technology, 2024, 152: 109363. DOI: 10.1016/j.ast.2024.109363.

[10] Wang Y, Wang H, Liu Y H, et al. 6-DOF UAV path planning and tracking control for obstacle avoidance: A deep learning-based integrated approach. Aerospace Science and Technology, 2024, 151: 109320. DOI: 10.1016/j.ast.2024.109320.

[11] Chai X, Zheng Z, Xiao J, et al. Multi-strategy fusion differential evolution algorithm for UAV path planning in complex environment. Aerospace Science and Technology, 2022, 121: 107287. DOI: 10.1016/j.ast.2021.107287.

[12] Fan J, Chen X, Liang X. UAV trajectory planning based on bi-directional APF-RRT* algorithm with goal-biased. Expert Systems with Applications, 2023, 213: 119137. DOI: 10.1016/j.eswa.2022.119137.

[13] Zhou X, Tang Z, Wang N, et al. A novel state transition algorithm with adaptive fuzzy penalty for multi-constraint UAV path planning. Expert Systems with Applications, 2024, 248: 123481. DOI: 10.1016/j.eswa.2024.123481.

[14] Jiang S, Wang J, Li C, et al. Identification of no-fly zones for delivery drone path planning in various urban wind environments. Physics of Fluids, 2024, 36(8): 085166. DOI: 10.1063/5.0221281.